Piezoelectric effect does not contribute in thermal drilling of quartz bearing rocks

Piezoelectric effect does not contribute in thermal drilling of quartz bearing rocks

T Saksala

Tampere University, Civil Engineering, PO Box 600, 33101-Tampere, Finland

timo.saksala@tuni.fi

Abstract. This paper presents a numerical study on a possible piezoelectric effect in thermal drilling of Quartz bearing rocks. For this end, the governing piezoelectro-thermo-mechanical problem is solved with the finite element method. The granitic rock material, consisting of Quartz, Feldspar and Biotite minerals, is taken as linear elastic but heterogeneous and anisotropic. Temperature dependence of material properties is neglected. The simulation demonstrates that the secondary stresses arising from converse piezoelectric effect are three orders of magnitude smaller than the primary thermal stresses, which means that the piezoelectric effect is negligible.

1. Introduction

Electrification effects, such as piezoelectricity and seismoelectricity, in rocks have important applications in the field of geophysical exploration. Moreover, piezoelectric properties and the thermal drillability of rocks containing piezoelectric minerals are interrelated to some extent [1]. Therefore, the drillability of, e.g Quartz bearing rocks, could be predicted based on their piezoelectric properties. Parkhomenko [1] hypothesised that there is an inverse secondary piezoelectric effect present in thermal drilling, accentuating the primary thermal stresses by secondary stresses arising from the electric charges due to thermal expansion of the quartz grains.

The principle of thermal drilling based on spallation phenomenon is illustrated schematically in Figure 1. Accordingly, when a rock surface is exposed to an intensive heating the resulting thermal gradient induces a compressive stress state, which leads to crack growth in the rock surface layer. When the cracks reach the critical length, spallation, i.e. ejection of rock chips, occurs. The minimal required temperature for spallation to occur in granitic rocks is about 500-600 °C [2]. Now, the Quartz grains in granite rock generate electric charges by the direct piezoelectric effect. This in turn, as hypothesised by Parkhomenko, accentuates the thermal stress states due to secondary piezoelectric stresses.

The present study addresses this topic by a numerical study. More specifically, the piezoelectric effect of Quartz is tested in rapid surface heating of a granite-like rock. For this end, a numerical method, based on finite elements, for solving the governing piezoelectro-thermo-mechanical problem is developed. The axisymmetric model, with the strong (local) form of the partial differential equations, is discretized with polygonal finite elements. Only the heat equation, having the external heat influx as the load term, depends on time and it is solved with the implicit Euler time integrator, while the quasi-static piezoelectric and mechanical balance equations are time independent. The

generic granite like rock is modelled as heterogeneous and anisotropic linear elastic material, and it consist of Quartz, Feldspar and Biotite minerals.

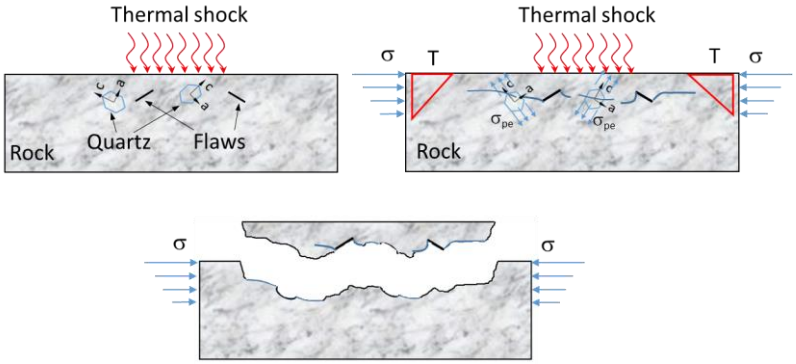

Figure 1. Principle of thermal spallation drilling of Quartz bearing rocks.

2. Theory of the modelling approach

The relevant theory of the modelling approach is described here. First, the strong form of the governing set of differential and constitutive equations is given. Then, the finite element discretized form and the solution method for the piezoelectro-thermo-mechanical problem is outlined. Finally, the heterogeneous and anisotropic description of rock material is detailed.

2.1. Strong form of the piezoelectro-thermo-mechanical problem

The strong form of equations governing the thermal drilling of piezoelectric rock are written as follows (tensor component notation):

$$\begin{cases} \rho c\dot{\theta} + q_{i,j} + Q = 0 \\ D_{i,i} - \rho_e = 0 \\ \sigma_{ij,j} - f_i^B = 0 \end{cases}$$
$$q_i = -k\theta_{,j}$$
$$\sigma_{ij} = C_{ijkl}(\varepsilon_{kl} - \alpha\Delta\theta\delta_{ij}) - e_{kij}E_k \quad (1)$$
$$D_i = e_{ikl}\varepsilon_{kl} - \varepsilon_{ij}^e E_k, \quad E_k = -\phi_{,k}$$

where symbols' meanings are as follows: ρ is the density; c is the specific heat capacity; θ is the temperature; q_i is the heat flux vector; Q is the term including mechanical heat production through dissipation and strain rate, which are ignored here as insignificant in comparison to external heat influx; D_i is the electric displacement; ρ_e is the electric charge; σ_{ij} is the stress tensor; f_i^B is the volume force vector; k is the thermal conductance; C_{ijkl} is the elasticity tensor; ε_{kl} is the mechanical strain tensor; α is the thermal expansion coefficient; δ_{ij} is the Knocker delta symbol; e_{kij} is the piezoelectric coupling tensor; E_k is the electric field vector; ε_{ij}^e is the dielectric constants tensor; ϕ is the electric potential.

The first three equations in (1) are the heat balance, electro-static balance, and the elasto-static balance equations while the rest of the equations are the constitutive equations for linear thermo-elasto-piezoelectric material. The rock damage and plasticity effects are thus ignored and only stresses arising from thermal and piezoelectric effects are considered in this study. Moreover, temperature dependence of the material properties is ignored for simplicity. It should be noted that the only time

dependent equation in (1) is the heat equation. This is a justified choice due to the fact that inertia effects are negligible in thermal drilling.

2.2. Finite element discretized form of the piezo-thermo-mechanical problem

The finite element form of the problem described in Eq. (1) can be derived in standard techniques [3, 4] and reads at time $t + \Delta t$ (ignoring the irrelevant terms):

$$\begin{aligned}
&\mathbf{C}_\theta \dot{\boldsymbol{\theta}}_{t+\Delta t} + \mathbf{K}_\theta \boldsymbol{\theta}_{t+\Delta t} = \mathbf{f}^\theta_{t+\Delta t} \\
&\mathbf{K}_{\mathrm{u}} \mathbf{u}_{t+\Delta t} + \mathbf{K}_{\mathrm{u}\theta}(\boldsymbol{\theta}_{t+\Delta t} - \boldsymbol{\theta}_0) + \mathbf{K}_{\mathrm{u}\phi} \boldsymbol{\phi}_{t+\Delta t} = \mathbf{0} \\
&\mathbf{K}_{\phi\mathrm{u}} \mathbf{u}_{t+\Delta t} + \mathbf{K}_\phi \boldsymbol{\phi}_{t+\Delta t} = \mathbf{0} \quad \text{with}
\end{aligned} \tag{2}$$

$$\mathbf{K}_{\mathrm{u}} = \mathbf{A}_{e=1}^{N_e} \int_{\Omega_e} \mathbf{B}_{\mathrm{u}}^{e,T} \mathbf{C}_{\mathrm{e}} \mathbf{B}_{\mathrm{u}}^{e} \mathrm{d}\Omega, \quad \mathbf{K}_{\mathrm{u}\theta} = \mathbf{A}_{e=1}^{N_e} \int_{\Omega_e} \alpha \mathbf{B}_{\mathrm{u}}^{e,T} \mathbf{C}_{\mathrm{e}} [\mathbf{1} \otimes \mathrm{I}_\theta] \mathrm{d}\Omega$$

$$\mathbf{K}_{\mathrm{u}\phi} = \mathbf{A}_{e=1}^{N_e} \int_{\Omega_e} \mathbf{B}_{\mathrm{u}}^{e,T} \mathbf{e} \mathbf{B}_{\phi}^{e} \mathrm{d}\Omega, \quad \mathbf{K}_{\phi\mathrm{u}} = \mathbf{K}_{\mathrm{u}\phi}^{\ T}$$

$$\mathbf{C}_\theta = \mathbf{A}_{e=1}^{N_e} \int_{\Omega_e} \rho c \mathbf{N}_\theta^{e,T} \mathbf{N}_\theta^{e} \mathrm{d}\Omega, \quad \mathbf{K}_\theta = \mathbf{A}_{e=1}^{N_e} \int_{\Omega_e} k \mathbf{B}_\theta^{e,T} \mathbf{B}_\theta^{e} \mathrm{d}\Omega$$

$$\mathbf{K}_\phi = \mathbf{A}_{e=1}^{N_e} \int_{\Omega_e} \mathbf{B}_\phi^{e,T} \boldsymbol{\varepsilon} \mathbf{B}_\phi^{e} \mathrm{d}\Omega, \quad \mathbf{f}^\theta = -\mathbf{A}_{e=1}^{N_e} \int_{\partial\Omega_e} q_n \mathbf{N}_\theta^{e,T} \mathrm{d}\partial\Omega$$

where the symbol meanings are as follows: $\mathbf{K}_{\mathrm{u}}$ is the stiffness matrix; $\mathbf{u}_{t+\Delta t}$ is the nodal displacement vector; $\boldsymbol{\theta}_{t+\Delta t}$ and $\boldsymbol{\theta}_0$ are the nodal temperature and initial temperature, respectively; $\boldsymbol{\phi}_{t+\Delta t}$ is the nodal electric potential; $\mathbf{C}_\theta$ and $\mathbf{K}_\theta$ are the capacitance and conductance matrices, respectively; $\mathbf{f}^\theta_{t+\Delta t}$ is the external heat flux vector; $\mathbf{A}$ is the standard finite element assembly operator; $\mathbf{B}_{\mathrm{u}}^{e}$ is the kinematic matrix (mapping the nodal displacement into element strains); $\mathbf{N}_\theta^{e}$ is the temperature interpolation matrix; q_n is the normal component of the heat flux; $\mathbf{B}_\theta^{e} = \mathbf{B}_\phi^{e}$ is the gradient of $\mathbf{N}_\theta^{e}$; $\mathbf{e}$ and $\boldsymbol{\varepsilon}$ are the piezoelectric coupling and dielectric constant matrices, respectively. Furthermore, in term $\mathbf{1} \otimes \mathrm{I}_\theta$, $\mathbf{1}$ is the Voigt version of the second order unit tensor and I_θ is a special operator which gives the average of a scalar field, the temperature in the present case, at the nodes of a finite element.

The solution of system (1) is as follows. First, the temperature is solved from the heat equation, as it does not depend on the other field variables in the present case, employing the backward Euler scheme for time discretization. Then, the electric potential is eliminated from the second equation by using the third equation. After, some algebra, the final solution scheme is as follows:

$$\begin{aligned}
&(\mathbf{C}_\theta + \Delta t \mathbf{K}_\theta) \boldsymbol{\theta}_{t+\Delta t} = \mathbf{C}_\theta \boldsymbol{\theta}_t + \Delta t \mathbf{f}^\theta_{t+\Delta t} \rightarrow \boldsymbol{\theta}_{t+\Delta t} \\
&(\mathbf{K}_{\mathrm{u}} - \mathbf{K}_{\mathrm{u}\phi} \mathbf{K}_\phi^{-1} \mathbf{K}_{\phi\mathrm{u}}) \mathbf{u}_{t+\Delta t} = -\mathbf{K}_{\mathrm{u}\theta}(\boldsymbol{\theta}_{t+\Delta t} - \boldsymbol{\theta}_0) \rightarrow \mathbf{u}_{t+\Delta t} \\
&\mathbf{K}_\phi \boldsymbol{\phi}_{t+\Delta t} = -\mathbf{K}_{\phi\mathrm{u}} \mathbf{u}_{t+\Delta t} \rightarrow \boldsymbol{\phi}_{t+\Delta t}
\end{aligned} \tag{3}$$

This system is solved in this order.

2.3. Heterogeneous and anisotropic rock material description

The numerical granitic rock, consisting of α-Quartz (33%), Feldspar (59%) and Biotite (8%), is described as heterogeneous anisotropic linear elastic material. The crystal systems for these minerals are trigonal (α-Quartz), triclinic (Plagioclase Feldspar) and monoclinic (Biotite) [5-8]. However, Biotite is considered here as pseudo-hexagonal and the hexagonal values measured by Alexandrov and Ryzhov [5] are used. The corresponding elasticity matrices and piezoelectric constants matrix $\mathbf{d}$ ($\mathbf{e} = \mathbf{C}_\mathrm{e}\mathbf{d}^\mathrm{T}$) for Quartz are in 2D axisymmetry [8]:

$$\mathbf{C}_e^q = \begin{pmatrix} C_{11} & C_{13} & 0 & C_{12} \\ C_{13} & C_{33} & 0 & C_{13} \\ 0 & 0 & \frac{1}{2}(C_{11}-C_{12}) & 0 \\ C_{12} & C_{13} & 0 & C_{11} \end{pmatrix}, \quad \mathbf{d}^q = \begin{pmatrix} d_{11} & 0 & 0 & -d_{11} \\ 0 & 0 & -2d_{11} & 0 \end{pmatrix} \tag{4}$$

$$\mathbf{C}_e^f = \begin{pmatrix} C_{11} & C_{13} & C_{16} & C_{12} \\ C_{13} & C_{33} & C_{36} & C_{23} \\ C_{16} & C_{36} & C_{66} & C_{26} \\ C_{12} & C_{23} & C_{26} & C_{22} \end{pmatrix}, \quad \mathbf{C}_e^b = \begin{pmatrix} C_{11} & C_{13} & 0 & C_{12} \\ C_{13} & C_{33} & 0 & C_{13} \\ 0 & 0 & \frac{1}{2}(C_{11}-C_{12}) & 0 \\ C_{12} & C_{13} & 0 & C_{11} \end{pmatrix} \tag{5}$$

where the coefficients numbering refers to the 3D elasticity tensor in Voigt's notation with the component ordering [11 22 33 23 13 12], while the ordering here is such that the terms corresponding to the hoop stress are on the 4th row and column.

The rock heterogeneity is described by random clusters of finite elements in the mesh so that each mineral is allotted the percentage of elements in the mesh corresponding to the percentage of each mineral in the rock.

3. Numerical examples

The numerical simulations of intensive surface heating of rock are carried out here. As mentioned, the rock heterogeneity is accounted for by random clusters of polygonal finite elements representing three different rock constituent minerals (see Figure 2). For the theory of polygonal finite elements and their application in numerical modelling of rock fracture, see Saksala and Jabareen [9]. The material properties for the minerals used in the simulations are given in Table 1 and 2.

Table 1. Elasticity constants for rock minerals in GPa [5-7]

Quartz	C_{11}	C_{33}	C_{12}	C_{13}	d_{11}*	
	87.3	105.8	6.6	12.0	2.27	
Biotite	C_{11}	C_{33}	C_{12}	C_{13}		
	186.0	54.0	32.4	11.6		
Feldspar	C_{11}	C_{22}	C_{33}	C_{66}	C_{12}	C_{13}
	104.8	190.1	169.3	35.6	50.2	42.2
	C_{16}	C_{23}	C_{26}	C_{36}		
	-4.3	18.6	-4.6	-5.2		

*Unit pC/N

Table 2. Material and model parameters for simulation.

Parameter/mineral	Quartz	Feldspar	Biotite
ρ [kg/m^3]	2650	2630	3050
α [1/K]	1.60E-5	0.75E-5	1.21E-5
k [W/mK]	4.94	2.34	3.14
c [J/kgK]	731	730	770
ε [F/m]	$4.5\varepsilon_0$	$6.3\varepsilon_0$	$7.75\varepsilon_0$

ε_0 = 8.854E-12 F/m

The boundary conditions and the finite element mesh are shown in Figure 2. The model surfaces are assumed thermally insulated. In order to make a "fair case" for the piezoelectric hypothesis, it is quite unrealistically assumed that all the Quartz grains, represented here by polygonal finite elements, are

left-handed and display a perfectly oriented texture with the mineral optical c-axis conforming to the global z-axis of the 2D axisymmetric coordinates. Finally, the heating time and the flux intensity are, respectively, specified as 1s and q_n = 1 MW/m^2. These values are chosen for demonstrative purposes only and they do not necessarily represent practical values.

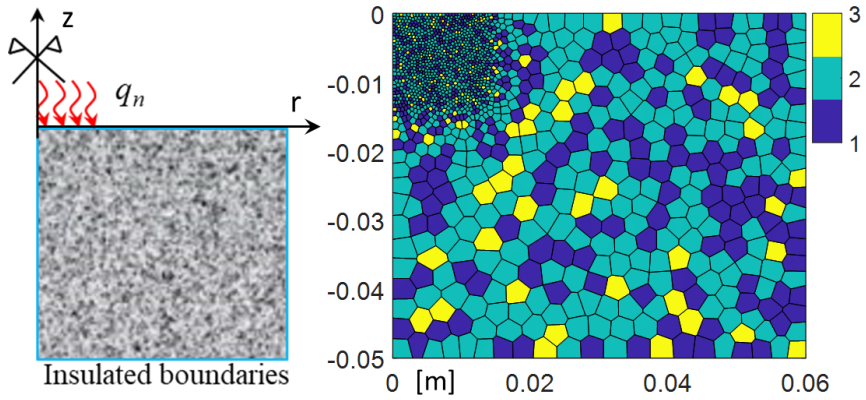

Figure 2. Boundary conditions and the finite element mesh (1500 polygons, 1 = Quartz, 2 = Feldspar, 3 = Biotite) for thermal shock simulations.

Simulation results are presented in Figure 3.

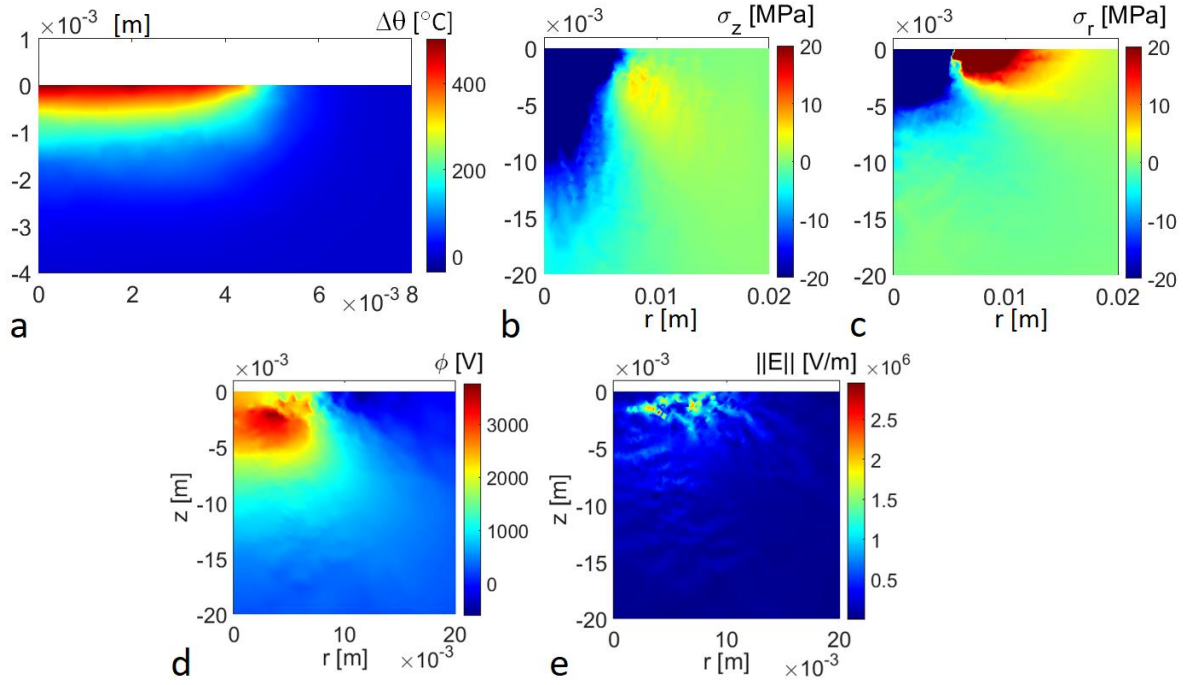

Figure 3. Simulation results for thermal surface shock (T = 1s, q_n = 1 MW/m^2): temperature (a), axial stress (c), radial stress (c), electric potential (d), and electric field strength (d) distribution at the end of simulation.

According to the results in Figure 3a, the temperature at the surface reaches 500 °C, i.e. the lower limit for spallation to occur. This high temperature naturally induces thermal stresses of extremely high magnitudes. The compressive stress in z-direction and the tensile stress in r-direction reach 700 MPa

and 100 MPa, respectively. Such tresses surely generate substantial charge via direct piezoelectric effect. Indeed, the maximum voltage induced is almost 4 kV (Figure 3d) and electric field strength exceeds 2.5E6 V/m at some locations (Figure 3e).

Now, if Equation $(2)_2$ is solved for displacement while neglecting the thermal coupling term and using the voltage in Figure 3d as a loading (converse piezoelectric effect) instead, the magnitude of the secondary stress field can be estimated. The values of radial and axial stresses thus solved barely reach 0.5 MPa, i.e. three orders of magnitude lower that the stresses induced by the thermal shock. The same result is obtained by inspection of the diagonal entries of matrices in the l.h.s of Equation $(3)_2$ $\mathbf{K}_{\mathrm{u}}$ and $\mathbf{K}_{\mathrm{u}\phi}\mathbf{K}_{\phi}^{-1}\mathbf{K}_{\phi\mathrm{u}}$ – the diagonal entries of the former are three orders of magnitude larger than those of the latter.

4. Conclusions

The numerical study on the possible piezoelectric effect of Quartz in thermal drilling of granite was presented. Despite the simplifying assumptions, i.e. linear elastic material with temperature independent material properties, the results suggest that piezoelectric effect has no role in thermal drilling. More precisely, the secondary stresses arising from converse piezoelectric effect in thermal drilling are three orders of magnitude smaller than the primary thermal stresses.

Acknowledgements

This research was funded by Academy of Finland under grant number 298345.

References

[1] Parkhomenko EI. 1971 Electrification Phenomena in Rocks. Springer, New York, 1971.
[2] Kant MA and von Rohr PR. 2016 Minimal Required Boundary Conditions for the Thermal Spallation Process, *Int J Rock Mech Min Sci*. Vol 84: 177-186.
[3] Ottosen NS, Ristinmaa M. 2005 The Mechanics of Constitutive Modeling, Elsevier, 2005.
[4] Allik H, Hughes TJR. 1970 Finite element method for piezoelectric vibration. *Int J Numer Methods Eng*. Vol 2: 151-157.
[5] Alexandrov KS, Ryzhova TV. 1961 Elastic properties of rock-forming minerals. II. Layered silicates, Izv. Acad. Sci. USSR Geophys. Ser., Engl. Transl. Vol 12:1165-1168.
[6] Brown JM, Angel RJ, Ross NL. 2016 Elasticity of plagioclase feldspars. *J. Geophys. Res. B: Solid Earth.* Vol 121: 663-675.
[7] Heyliger P. Ledbetter H, Kim S. 2003 Elastic constants of natural quartz. *J. Acoust. Soc. Am*. Vol 114: 644-650.
[8] Newnham RE. 2005 Properties of Materials: Anisotropy, Symmetry, Structure. Oxford University Press, New York, 2005.
[9] Saksala T, Jabareen M. 2019 Numerical modelling of rock fracture under dynamic loading with polygonal finite elements. *Int J Numer Anal Methods Geomech*. Vol 43:2056–2074.